Princeton Plasma Physics Laboratory

PPPL-5176

Ion Temperature Effects on Magnetotail Alfven Wave Propagation and Electron Energization

P.A. Damiano[1], J.R. Johnson[1], and C.C. Chaston[2,3]
1 Princeton Center for Heliophysics, Princeton Plasma Physics Laboratory, Princeton University, Princeton, NJ 08543
2 Space Sciences Laboratory, University of California, Berkeley, CA 94720
3 School of Physics, University of Sydney, Sydney, NSW 2006, Australia

January 2015

Prepared for the U.S. Department of Energy under Contract DE-AC02-09CH11466.

Princeton Plasma Physics Laboratory
Report Disclaimers

Full Legal Disclaimer

This report was prepared as an account of work sponsored by an agency of the United States Government. Neither the United States Government nor any agency thereof, nor any of their employees, nor any of their contractors, subcontractors or their employees, makes any warranty, express or implied, or assumes any legal liability or responsibility for the accuracy, completeness, or any third party's use or the results of such use of any information, apparatus, product, or process disclosed, or represents that its use would not infringe privately owned rights. Reference herein to any specific commercial product, process, or service by trade name, trademark, manufacturer, or otherwise, does not necessarily constitute or imply its endorsement, recommendation, or favoring by the United States Government or any agency thereof or its contractors or subcontractors. The views and opinions of authors expressed herein do not necessarily state or reflect those of the United States Government or any agency thereof.

Trademark Disclaimer

Reference herein to any specific commercial product, process, or service by trade name, trademark, manufacturer, or otherwise, does not necessarily constitute or imply its endorsement, recommendation, or favoring by the United States Government or any agency thereof or its contractors or subcontractors.

PPPL Report Availability

Princeton Plasma Physics Laboratory:

http://www.pppl.gov/techreports.cfm

Office of Scientific and Technical Information (OSTI):

http://www.osti.gov/scitech/

Related Links:

U.S. Department of Energy

U.S. Department of Energy Office of Science

U.S. Department of Energy Office of Fusion Energy Sciences

Ion temperature effects on magnetotail Alfvén wave propagation and electron energization

P.A. Damiano,[1] J.R. Johnson[1] and C.C. Chaston[2,3]

[1]Princeton Center for Heliophysics,

Princeton Plasma Physics Laboratory,

Princeton University, Princeton, NJ 08543

[2]Space Sciences Laboratory, University of

California, Berkeley, CA 94720

[3]School of Physics, University of Sydney,

Sydney, NSW 2006, Australia

Abstract.

A new 2D self-consistent hybrid gyrofluid-kinetic electron model in dipolar coordinates is presented and used to simulate dispersive scale Alfvén wave pulse propagation from the equator to the ionosphere along an $L = 10$ magnetic field line. The model is an extension of the hybrid MHD-kinetic electron model [*Damiano et al.*, 2007] that incorporates ion Larmor radius corrections via the kinetic fluid model of *Cheng and Johnson* [1999]. It is found that consideration of a realistic ion to electron temperature ratio decreases the propagation time of the wave from the plasma sheet to the ionosphere by several seconds relative to a $\rho_i = 0$ case (which also implies shorter timing for a substorm onset signal) and leads to significant dispersion of wave energy perpendicular to the ambient magnetic field. Additionally, ion temperature effects reduce the parallel current and electron energization all along the field line for the same magnitude perpendicular electric field perturbation.

1. Introduction

The formation of the broadband aurora, which are seen to increase rapidly at substorm onset [e.g. *Wing et al.*, 2013], have been linked to electron precipitation associated with dispersive scale Alfvén waves - waves with perpendicular scale lengths on the order of λ_e, ρ_s and ρ_i [*Keiling et al.*, 2003]. How electrons interact with these waves is dictated by the location of the wave along the field line. Close to the ionospheric boundary, $\beta \ll m_e/m_i$, electron inertial effects dominate and electrons can be energized by Fermi acceleration processes [e.g. *Kletzing*, 1994; *Chaston et al.*, 2000; *Watt and Rankin*, 2009]. Toward the plasma sheet, waves are in the kinetic Alfvén wave regime ($\beta \gg m_e/m_i$) and can couple to electrons which have parallel velocities close to the phase speed of the wave [e.g. *Watt and Rankin*, 2009]. In this latter region, ion gyroradius effects are expected to play an important role because in the plasma sheet $T_i/T_e \sim 7$ [*Baumjohann et al.*, 1989] which implies that ρ_i effects will control the phase speed of the wave, which affects both the propagation time of the wave from an onset site to the ionosphere [e.g. *Lessard et al.*, 2006; *Chi et al.*, 2009] and the resonance condition necessary for electron acceleration. Additionally, ρ_i is an important scale length associated with the cross scale coupling of wave energy to kinetic scales through a turbulent cascade [*Chaston et al.*, 2008].

Although there is a significant body of previous simulation work devoted to electron acceleration by dispersive scale waves [*Kletzing*, 1994; *Chaston et al.*, 2000; *Chaston et al.*, 2002; *Watt et al.*, 2004; *Damiano and Wright*, 2005; *Watt et al.*, 2006; *Watt and Rankin*, 2009] attention to ion gyroradius effects has been relatively limited to studies involving gyrofluid approaches without self consistent coupling to kinetic electrons (e.g. *Su et al.*

[2006] and *Jones and Su* [2008], in application to Jovian aurora, and *Streltsov et al.* [1998] in application to terrestrial Field Line Resonances) or Particle-In-Cell treatments [*Shay et al.*, 2011] that, although considering all the relevant physics, are restricted to more localized studies in the plasma sheet due to the computational costs of considering the full orbital dynamics of all the particles.

With this motivation in mind, we have adapted a 2D hybrid MHD-kinetic electron model in curvilinear coordinates [*Damiano et al.*, 2007; *Damiano and Wright*, 2008], which has been used extensively to consider electron acceleration in geomagnetic Field Line Resonances, to include ion gyroradius effects using the kinetic-fluid model of *Cheng and Johnson* [1999]. The model is used to simulate kinetic Alfvén wave propagation from an equatorial source region in the magnetotail (where these waves are ubiquituous within about 15 R_E, asssociated with the breaking of reconnection induced fast flows - *Chaston et al.* [2012]) to the ionospheric boundary of the simulation domain. The rest of the paper is broken up into four sections. Section 2 summarizes the hybrid model used. Section 3 presents the simulation results while Section 4 gives our conclusions.

2. Gyrofluid-Kinetic-Electron Model

The simulations were conducted with the new 2-D Gyrofluid-Kinetic Electron (GKE) model in dipolar coordinates, which is the gyrofluid extension of the hybrid MHD-kinetic electron model [*Damiano et al.*, 2007] that has been used primarily to date to investigate electron dynamics in geomagnetic Field Line Resonances [*Damiano et al.*, 2007; *Damiano and Wright*, 2008; *Damiano and Johnson*, 2012]. The model treats electron motion along field lines as drift-kinetic, and ions with a kinetic-fluid closure based on a solution of the linear gyrokinetic equation [*Cheng and Johnson*, 1999], which includes ion Larmor radius corrections as well as the physics of the ion polarization current. The model geometry is illustrated in Figure 1a and explicitly includes the field aligned direction (x_1) and the direction across L shells (x_2). The system is independent of the azimuthal coordinate so that $\partial/\partial x_3 = 0$. In denoting the component electron velocities we will also use the notation $v_{||} = v_1$ and $v_\perp = \sqrt{v_2^2 + v_3^2}$ to indicate the gyrophase independent perpendicular velocity.

Consistent with the Field Line Resonance studies presented in *Damiano and Wright* [2008] and *Damiano and Johnson* [2012, 2013], the simulation grid used in this analysis is 0.6 R_E wide at the equator and the ionospheric boundaries are set to a geocentric altitude of 2 R_E. This altitude corresponds to the average location of the B/n peak (where the peak electron acceleration is believed to occur [*Wright et al.*, 2002; *Damiano and Wright*, 2008]) and the width of the grid tapers down to about 100 km at this altitude [*Damiano and Johnson*, 2013]. In this topology, the perpendicular scale lengths of the kinetic Alfvén waves imposed at the equator (as discussed later in the section), naturally taper down to electron inertial scales close to the ionospheric boundary.

The gyrofluid portion of the model incorporates the modified linearized momentum equation given by

$$\mu_o \rho_o \frac{\partial \tilde{u}_3}{\partial t} = \frac{B_o}{h_1 h_3} \left(\frac{\partial}{\partial x_1} (h_3 b_3) \right) \tag{1}$$

where the ion gyroradius (ρ_i) response is included via the perpendicular pressure term which can be expressed in the form of a modified velocity given by $\tilde{u}_3 = (1 - 1.25\rho_i^2 \nabla_\perp^2) u_3$. The coefficients of $\rho_i^2 \nabla_\perp^2$ here are obtained using a Padé approximation [*Johnson and Cheng*, 1997; *Cheng and Johnson*, 1999]. This equation is coupled to Faraday's law

$$\frac{\partial b_3}{\partial t} = \frac{-1}{h_1 h_2}\left(\frac{\partial}{\partial x_1}(h_2 E_2) - \frac{\partial}{\partial x_2}(h_1 E_1)\right) \tag{2}$$

and the perpendicular (where Padé approximants have also been used)

$$E_2 = -B_o(1 - \rho_i^2 \nabla_\perp^2)\tilde{u}_3 \tag{3}$$

and parallel Ohm's laws

$$\begin{aligned}
\frac{\partial}{\partial x_2}\left(\frac{h_3}{h_1 h_2}\left(\frac{\partial h_1 E_1}{\partial x_2}\right)\right) - \frac{h_1 E_1}{\lambda_e^2} &= \frac{\partial}{\partial x_2}\left(\frac{h_3}{h_1 h_2}\frac{\partial}{\partial x_1}(h_2 E_2)\right) \\
&+ e\mu_o \frac{\partial}{\partial x_1}\int v_1^2 f d^3v \\
&+ \mu_o \frac{e}{m_e}\frac{\partial B_o}{\partial x_1}\int \mu_m f d^3v \\
&- 2\mu_o \frac{e}{m_e}\frac{\partial B_o}{\partial x_1}\int \frac{m_e v_1^2}{2B_o} f d^3v
\end{aligned} \tag{4}$$

where $x_1 = \cos\theta/r^2$, $x_2 = \sin^2\theta/r$, $x_3 = \phi$, $h_1 = r^3/(1+3\cos^2\theta)^{1/2}$, $h_2 = r^2/(\sin\theta(1+3\cos^2\theta)^{1/2})$, and $h_3 = r\sin\theta$. A similar gyrofluid closure was also used in the two fluid model of *Streltsov et al.* [1998]. In equation (4), $\lambda_e = \sqrt{m_e/\mu_o n e^2}$ is the electron inertial length, $\mu_m = m_e v_\perp^2/(2B)$ is the electron magnetic moment, the second term on the right hand side relates to the parallel gradient of the electron pressure while the third and fourth terms incorporate the perpendicular and parallel electron pressures.

Parallel electron dynamics are described by the guiding center equations

$$m_e \frac{dv_1}{dt} = -eE_1 - \mu_m \frac{1}{h_1}\frac{\partial B_o}{\partial x_1} \tag{5}$$

$$h_1 \frac{dx_1}{dt} = v_1 \tag{6}$$

where $v_1 = v_{||}$ is the parallel electron velocity and the integral moments of the electron distribution function used in the parallel Ohm's law are computationally treated as summations using standard Particle-In-Cell techniques as discussed in *Damiano et al.* [2007].

For the present simulations, electrons are initially positioned to form a constant density such that $n_e = n_i = 1$ cm^{-3} (which yields $\lambda_e \approx 5$ km) and a uniform electron distribution is assumed in velocity space. Perfectly conducting boundary conditions are assumed at the ionospheres, while at the perpendicular boundaries (along the lines of constant x_2) a node in current is imposed.

Equations (1) to (3) with $E_1 = 0$ are a self-consistent set of equations which incorporates ion gyroradius effects on Alfvén wave propagation, but neglects kinetic electron physics. In a cartesian geometry with uniform plasma parameters, these equations, along with a parallel momentum equation including electron temperature effects, yield a dispersion relation of the form:

$$\omega = k_{||} V_A \sqrt{1 + k_\perp^2 \rho_i^2 (1 + \frac{T_e}{T_i})} \tag{7}$$

where, as a result of the use of Padé approximants [e.g. see *Johnson and Cheng*, 1997; *Streltsov et al.*, 1998; *Cheng and Johnson*, 1999], this expression provides a uniform approximation to the analytical dispersion relation [e.g. see *Hasegawa*, 1976; *Lysak and Lotko*, 1996] on all scales to within an accuracy of 6% [*Streltsov et al.*, 1998]. As such, it is preferable to the commonly used small or large scale expansions and will be used in the analysis of the some of the simulation data to follow.

Waves are launched by a perturbation of azimuthal velocity, applied at t=0, which corresponds to the initial perpendicular electric field shown in Figure 1b. This is equivalent to perturbing the ion polarization current. The amplitude of the E_2 profile is chosen to be order of magnitude comparable with observations [e.g. *Keiling*, 2009] and the wave perturbation is centered in the equatorial plane, where we assume a parallel Gaussian profile with a Full-Width-Half Max of 1 R_E and a perpendicular scale length (for a majority of this study) of 0.1 R_E (which yields $k_\perp \rho_i \sim 1$ for $T_i = 1$ keV and the resulting ratio $k_\perp / k_{||} \sim 10$ is within the range evident in the observations of *Chaston et al.* [2014]). This perturbation results in identical Alfvén wave pulses propagating toward the opposing ionospheric boundaries (with both upward and downward parallel current characteristics). For the purposes of this study, we focus on the pulse propagating toward the northern ionosphere (upper half plane of Figure 1a) carrying an upward directed field aligned current (along the field line denoted by the dotted line in the Figure 1b).

3. Simulations

The electron distribution function is initialized with a temperature of 100 eV, and we assume an ambient ion temperature of 1 keV which yields the field aligned profile of ρ_i displayed in Figure 2a. The resulting ratio of $T_e/T_i = 1/10$ is roughly consistent with the average temperature ratio of 1/7 measured in the plasma sheet [e.g. *Baumjohann et al.*, 1989]. Figure 2b illustrates the field-aligned Alfvén velocity profile and the horizontal line $v_{th} = V_A$ (where $v_{th} = \sqrt{2T_e/m_e}$) denotes the transition between the kinetic (KAW) and inertial (IAW) Alfvén wave regimes along the field line.

In order to make a consistent comparison between the $T_i = 0$ ($\rho_i = 0$) and the $T_i = 1$ keV cases, we initialized both systems so that the profiles and magnitudes of the perpendicular electric field, E_2, were consistent. The pulse profile in the $T_i = 1$ keV case is moving with a higher speed and also has a reduced amplitude relative to the $T_i = 0$ case. In Figure 3b, the equatorial perpendicular scale length has been reduced to 0.05 R_E (further increasing $k_\perp \rho_i$) and the wave phase speed is further increased and the current amplitude further reduced when compared to Figure 3a and the $T_i = 0$ case.

The increased phase speed is in agreement with what would be expected from the kinetic Alfvén wave dispersion relation, which (neglecting electron inertial effects) is given by equation 7. Since, $T_e \ll T_i$, we can ignore the last term in the brackets, and since $\lambda_\perp \sim 0.1$ R_E and $\rho_i \sim 100$ km at the equator, $k_\perp \rho_i = 2\pi\rho_i/\lambda_\perp \sim 1$ and the dispersion relation reduces to $\omega/k_{||} \sim \sqrt{2}V_A$. As ρ_i and $\lambda_\perp$ do not vary substantially between the equator and $l_{||} = 1.5$ R_E, this difference in velocity is roughly consistent with the different propagation distances evident between the two cases in Figure 3a given the same propagation times.

The reduction in the parallel current density between the cases displayed in Figure 3 can be understood from the cartoon inset in Figure 3b. The large gyroradius associated with a hot ion temperature will, see a reduced orbit averaged perpendicular electric field [*Tatsuno et al.*, 2009] and will consequently experience a reduced $< \vec{E} > \times \vec{B}$ drift and polarization current relative to a cold ion with a gyroradius close to the perpendicular scale length of the wave perturbation. The reduced polarization current associated with the hot ion will consequently need to be closed by a reduced parallel current (and hence a reduced $E_{||}$ to accelerate electrons). Essentially, hot ions do not respond to the field as easily and this system must be driven harder to yield a similar parallel current relative to the $T_i = 0$ case.

The reduction of $E_{||}$ can also be seen from a linear analysis of the two fluid equations where the ratio of the parallel and perpendicular electric fields in the limit of the kinetic Alfvén wave is approximated by the expression [e.g. *Chaston et al.*, 2003; *Streltsov et al.*, 1998]

$$E_{||}/E_{\perp} = \frac{-k_{||}k_{\perp}\rho_s^2}{(1 + k_{\perp}^2\rho_i^2)} \quad (8)$$

and for a finite electron temperature, this ratio decreases with increase in the size of the ion gyrodius (or increase in T_i). The corresponding reduction of $j_{||}$ can also be inferred from the equivalent expression for $E_{\perp}/b_{\perp}$ (e.g. equation (48) of *Stasiewicz et al.* [2000]). Also consistent with this analytical description, the magnitude of $E_{||}$ was significantly reduced in the high-altitude, near-equatorial plasma sheet region in two fluid simulations of Field Line Resonances when ρ_i effects were considered [*Streltsov et al.*, 1998].

The different phase speeds of the waves in the two cases considered, implies that we must superimpose the results at two different times in order to compare the evolution of the electron distribution function. Figure 4a super-imposes the profiles of the two runs so that the current maxima are centered at $l_{||} = 5\ R_E$, and Figures 4b and 4c respectively illustrate the corresponding electron distribution function measured at the same location. In Figure 4b, at low energies, the initialized distribution has evolved to become elongated in the parallel direction at lower energies while maintaining the symmetry of the original Maxwellian distribution at higher energies. These characteristics of the distribution function are qualitatively consistent with what is evident in both observations [e.g *Wygant* *et al.*, 2002; *Janhunen et al.*, 2004] and simulations [e.g. *Watt and Rankin*, 2009, 2012]. As with *Watt and Rankin* [2009, 2012], when the driving electric field is increased, the parallel asymmetry increases. However, in contrast to these other simulation efforts, we have not time averaged the distribution function to better correspond to the observations and we have used only a single pulse perturbation rather than the wave train that was considered in the studies of *Watt and Rankin* [2009, 2012].

The parallel elongation of the distribution function at low energy is the result of two factors; the parallel drift of a portion of the distribution function to carry the parallel current and the plateauing of the distribution function associated with Landau damping effects [e.g. *Watt and Rankin*, 2009]. The magnitude of the parallel drift will be proportional to the magnitude of the parallel current while the plateauing will occur around the phase speed of the wave. In the limit of $\rho_i = 0$, this velocity is on the order of the Alfvén speed which at $l_{||} = 5\ R_E \sim 1 \times 10^6$ m/s.

The reduction of the parallel current with the inclusion of ρ_i effects explains the reduced parallel elongation of the distribution function in Figure 4c relative to Figure 4b as the reduced current requires less particle drift to carry it and the reduced wave amplitude means that the width of the plateau associated with Landau damping effects is also reduced. The increased phase speed of the wave, relative to the $T_i = 0$ case, moves the resonance region very slightly toward the tail of the distribution, although it is not visible because this is completely lost in the core of the distribution function evident in Figure 4c. A more detailed analysis of ρ_i effects on the electron distribution function evolution will be left to a subsequent publication where we will explore a range of wave parameters.

Another consequence of including ρ_i effects is evident in Figure 4d which displays the perpendicular profile evident at $l_{||} = 5\ R_E$. The wave perturbation has become significantly broader in the $T_i = 1$ keV case (even though this case is plotted at an earlier time) due to the perpendicular dispersion of wave energy associated with ion gyroradius effects. This broadening means that more significant electron acceleration occurs along adjacent field lines compared with the original perturbation in order to carry the parallel current. Strictly speaking, the wave profile also broadens in the $T_i = 0$ case because of electron pressure effects, but since $T_i \gg T_e$, the ion temperature effects dominate the characteristics of the wave dispersion in the latter case. For $l_{||} \geq 8\ R_E$ (refer to Figure 2b), electron inertial effects dominate. However, the broadening associated with these effects is also too small to significantly modify the perpendicular profile established by ρ_i effects in the KAW regime.

Finally, Figure 5a displays the profile of parallel current at the ionospheric boundary as a function of time. Consistent with the previous Figures 3 and 4c, the ionospheric magnitude of the parallel current in the $T_i = 1$ keV case is significantly reduced relative to the $T_i = 0$ case. This reduced current is reflected in the diminished high energy tail, in the $T_i = 1$ keV case, illustrated in Figure 5b. This result confirms that even though the peak of the electron energization is occurring at this altitude (where the imposed perpendicular perturbations naturally taper to λ_e scales), the ρ_i effects dominant in the plasma sheet limit the extent of the energization. Additionally, the maximum in the parallel current density occurs about 7 seconds earlier in the $T_i = 1$ keV ($t \approx 30$ s) case due to the increased phase speed of the wave relative to the $T_i = 0$ case ($t \approx 37$ s). Although the "ionospheric boundary" in the simulation is high relative to the Earth (in order to reduce computational costs), the propagation times predicted would not be greatly changed if we further reduced the altitude of the ionosphere in the model because the transit time is primarily constrained by slower wave propagation in the plasma sheet. By the time the wave reaches close to the ionosphere, the phase speed $\sim 10^8$ m/s and so propagation through the remaining R_E to the realistic ionospheric altitude only adds a fraction of a second to the propagation time. When the ion temperature was further increased to 5 keV, the peak in the ionospheric parallel current occurred significantly earlier still at $t = 15$ seconds, although the amplitude is much smaller because $k_\perp \rho_i$ is larger.

Figure 5a also illustrates a longer temporal width to the pulse ionospheric signature in the $T_i = 1$ keV case relative to the $T_i = 0$ case. This increase is simply due to the fact that (from equation 7) the dependence of the phase speed on $k_\perp \rho_i$ (which increases as the ionospheric boundary is approached) leads to a greater velocity difference between the leading and trailing edges of the pulse relative to the $T_i = 0$ case.

4. Conclusions

In this work, we have studied the propagation of a kinetic Alfvén wave pulse from the magnetotail to the ionosphere using a new self consistent Gyrofluid-Kinetic Electron model (GKE) in a dipolar topology and have explored how ion gyroradius effects modify the propagation characteristics of the pulse and the associated electron energization. While magnetotail kinetic Alfvén wave propagation has been considered previously in the context of kinetic simulations, we believe that this is the first effort to do so in a 2D dipolar topology propagating a pulse all the way from the plasma sheet to the ionosphere. It is found that the inclusion of ρ_i effects results in a significantly faster propagation time for the pulse from the plasmasheet to the ionosphere. For a KAW perturbation with $\lambda_{\perp_{eq}} = 0.1\ R_E$ (along an $L = 10$ field line), and assuming $T_e = 100$ eV and $T_i = 1$ keV (resulting in a value of $k_\perp \rho_i \sim 1$ in the plasma sheet), the parallel current maximizes at the ionosphere about 7 seconds earlier relative to the $T_i = 0$ case. This time difference increases with larger $k_\perp \rho_i$. The inclusion of ρ_i effects also results in an increased dispersion of wave energy perpendicular to the ambient magnetic field relative to the $\rho_i = 0$ case.

In addition to the increased phase speed and dispersion as $k_\perp \rho_i$ increases, the resulting $j_\parallel$ (and hence electron energization) is reduced for a given magnitude of the perpendicular electric field (even though the primary electron acceleration is taking place in the region above ionospheric boundary where λ_e effects dominate). This reduction occurs because a hot ion will, on average, see a reduced average perpendicular electric field relative to a colder counterpart, resulting in a reduced $\vec{E} \times \vec{B}$ drift and ion polarization current. This reduced polarization current requires a reduced parallel current for closure and a correspondingly reduced electron energization to carry the parallel current (which is qualitatively consistent with the results of *Chaston et al.* [2003]).

Finally, while some of the ρ_i effects on magnetospheric Alfvén waves discussed here can be derived from a gyrofluid description alone, such studies miss the all important self-consistent coupling to kinetic electrons which is crucial to improve our understanding of the electron energization and wave damping. Therefore, the model presented here is an important advancement to gyrofluid descriptions alone and we will use it to further explore the details of the wave-electron interactions for a range of realistic wave and plasma parameters in a follow-up investigation.

Acknowledgments. The authors acknowledge support from NASA grants (NNH11AR071, NNH09AM53I, and NNH09AK63I) and NSF grants (ATM0902730 and AGS1203299). C. Chaston also acknowledges support from Australian Research Council grant No. FT110100316. This manuscript was authored by Princeton University under Contract Number DE-AC02-09CH11466 with the U.S. Department of Energy. This work was facilitated by the Max-Planck/Princeton Center for Plasma Physics. The United States Government retains a non-exclusive, paid-up, irrevocable, world-wide license to publish or reproduce the published form of this manuscript, or allow others to do so, for United States Government purposes. The numerical data used in the figures may be obtained by contacting the corresponding author.

References

Baumjohann, W., G. Paschmann, and C. A. Cattell (1989), Average plasma properties in the central plasma sheet, *J. Geophys. Res.,* , *94*, 6597–6606, doi: 10.1029/JA094iA06p06597.

Chaston, C. C., C. W. Carlson, R. E. Ergun, and J. P. McFadden (2000), Alfvén Waves, Density Cavities and Electron Acceleration Observed from the FAST Spacecraft, *Physica Scripta Volume T*, *84*, 64–68, doi:10.1238/Physica.Topical.084a00064.

Chaston, C. C., J. W. Bonnell, L. M. Peticolas, C. W. Carlson, J. P. McFadden, and R. E. Ergun (2002), Driven alfvén waves and electron acceleration, *Geophys. Res. Lett.*, *29*, 1535.

Chaston, C. C., J. W. Bonnell, C. W. Carlson, J. P. McFadden, R. J. Strangeway, and R. E. Ergun (2003), Kinetic effects in the acceleration of auroral electrons in small scale Alfven waves: A FAST case study, *Geophys. Res. Lett.*, , *30*, 1289, doi:10.1029/2002GL015777.

Chaston, C. C., C. Salem, J. W. Bonnell, C. W. Carlson, R. E. Ergun, R. J. Strangeway, and J. P. McFadden (2008), The Turbulent Alfvénic Aurora, *Physical Review Letters*, *100*(17), 175,003–+, doi:10.1103/PhysRevLett.100.175003.

Chaston, C. C., J. W. Bonnell, L. Clausen, and V. Angelopoulos (2012), Energy transport by kinetic-scale electromagnetic waves in fast plasma sheet flows, *Journal of Geophysical Research (Space Physics)*, *117*, A09202, doi:10.1029/2012JA017863.

Chaston, C. C., J. W. Bonnell, and C. Salem (2014), Heating of the Plasma Sheet by Broadband Electromagnetic Waves, *Geophysical Research Letters*, doi: 10.1002/2014GL062116.

Cheng, C. Z., and J. R. Johnson (1999), A kinetic-fluid model, *J. Geophys. Res.*, *104*, 413–428, doi:10.1029/1998JA900065.

Chi, P. J., C. T. Russell, and S. Ohtani (2009), Substorm onset timing via traveltime magnetoseismology, *Geophys. Res. Lett.*, , *36*, L08107, doi:10.1029/2008GL036574.

Damiano, P. A., and J. R. Johnson (2012), Electron acceleration in a geomagnetic Field Line Resonance, *Geophys. Res. Lett.*, , *39*, L02102, doi:10.1029/2011GL050264.

Damiano, P. A., and J. R. Johnson (2013), Mirror force induced wave dispersion in Alfvén waves, *Physics of Plasmas*, *20*(6), 062,901, doi:10.1063/1.4810788.

Damiano, P. A., and A. N. Wright (2005), Two-dimensional hybrid MHD-kinetic electron simulations of an Alfvén wave pulse, *Journal of Geophysical Research (Space Physics)*, *110*, A01201, doi:10.1029/2004JA010603.

Damiano, P. A., and A. N. Wright (2008), Electron thermal effects in standing shear Alfvén waves, *Journal of Geophysical Research (Space Physics)*, *113*, A09219, doi:

10.1029/2008JA013087.

Damiano, P. A., A. N. Wright, R. D. Sydora, and J. C. Samson (2007), Energy dissipation via electron energization in standing shear Alfvén waves, *Phys. Plasmas*, *14*, 062,904.

Hasegawa, A. (1976), Particle acceleration by MHD surface wave and formation of aurora, *J. Geophys. Res.*, *81*, 5083–5090, doi:10.1029/JA081i028p05083.

Janhunen, P., A. Olsson, J. Hanasz, C. Russell, H. Laakso, and J. Samson (2004), Different Alfvén wave acceleration processes of electrons in substorms at ~4-5 RE and 2-3 RE radial distance, *Annales Geophysicae*, *22*, 2213–2227, doi:10.5194/angeo-22-2213-2004.

Johnson, J. R., and C. Z. Cheng (1997), Kinetic Alfvén waves and plasma transport at the magnetopause, *Geophys. Res. Lett.*, *24*, 1423–1426, doi:10.1029/97GL01333.

Jones, S. T., and Y.-J. Su (2008), Role of dispersive Alfvén waves in generating parallel electric fields along the Io-Jupiter fluxtube, *Journal of Geophysical Research (Space Physics)*, *113*, A12205, doi:10.1029/2008JA013512.

Keiling, A. (2009), Alfvén Waves and Their Roles in the Dynamics of the Earth's Magnetotail: A Review, *Space Science Review*, *142*, 73–156, doi:10.1007/s11214-008-9463-8.

Keiling, A., J. R. Wygant, C. A. Cattell, F. S. Mozer, and C. T. Russell (2003), The Global Morphology of Wave Poynting Flux: Powering the Aurora, *Science*, *299*, 383–386, doi:10.1126/science.1080073.

Kletzing, C. A. (1994), Electron acceleration by kinetic Alfvén waves, *J. Geophys. Res.*, *99*, 11,095–11,104, doi:10.1029/94JA00345.

Lessard, M. R., E. J. Lund, S. L. Jones, R. L. Arnoldy, J. L. Posch, M. J. Engebretson, and K. Hayashi (2006), Nature of Pi1B pulsations as inferred from ground and satellite observations, *Geophys. Res. Lett.*, , *33*, L14108, doi:10.1029/2006GL026411.

Lysak, R., and W. Lotko (1996), On the kinetic dispersion relation for shear Alfvén waves, *J. Geophys. Res.*, *101*, 5085.

Shay, M. A., J. F. Drake, J. P. Eastwood, and T. D. Phan (2011), Super-Alfvénic Propagation of Substorm Reconnection Signatures and Poynting Flux, *Physical Review Letters*, *107*(6), 065001, doi:10.1103/PhysRevLett.107.065001.

Stasiewicz, K., et al. (2000), Small Scale Alfvénic Structure in the Aurora, *Space Science Reviews*, *92*, 423–533.

Streltsov, A. V., W. Lotko, J. R. Johnson, and C. Z. Cheng (1998), Small-scale, dispersive field line resonances in the hot magnetospheric plasma, *J. Geophys. Res.*, , *103*, 26,559–26,572, doi:10.1029/98JA02679.

Su, Y.-J., S. T. Jones, R. E. Ergun, F. Bagenal, S. E. Parker, P. A. Delamere, and R. L. Lysak (2006), Io-Jupiter interaction: Alfvén wave propagation and ionospheric Alfvén resonator, *Journal of Geophysical Research (Space Physics)*, *111*, A06211, doi:10.1029/2005JA011252.

Tatsuno, T., W. Dorland, A. A. Schekochihin, G. G. Plunk, M. Barnes, S. C. Cowley, and G. G. Howes (2009), Nonlinear Phase Mixing and Phase-Space Cascade of Entropy in Gyrokinetic Plasma Turbulence, *Physical Review Letters*, *103*(1), 015003, doi:10.1103/PhysRevLett.103.015003.

Watt, C. E. J., and R. Rankin (2009), Electron Trapping in Shear Alfvén Waves that Power the Aurora, *Physical Review Letters*, *102*(4), 045002, doi:10.1103/PhysRevLett.102.045002.

Watt, C. E. J., and R. Rankin (2012), Alfvén Wave Acceleration of Auroral Electrons in Warm Magnetospheric Plasma, *Washington DC American Geophysical Union Geo-*

physical Monograph Series, *197*, 251–260, doi:10.1029/2011GM001171.

Watt, C. E. J., R. Rankin, and R. Marchand (2004), Kinetic simulations of electron response to shear alfvén waves in magnetospheric plasmas, *Phys. Plasmas*, *11*, 1277.

Watt, C. E. J., R. Rankin, I. J. Rae, and D. M. Wright (2006), Inertial Alfvén waves and acceleration of electrons in nonuniform magnetic fields, *Geophys. Res. Lett.*, *33*, L02,106.

Wing, S., M. Gkioulidou, J. R. Johnson, P. T. Newell, and C.-P. Wang (2013), Auroral particle precipitation characterized by the substorm cycle, *Journal of Geophysical Research (Space Physics)*, *118*, 1022–1039, doi:10.1002/jgra.50160.

Wright, A. N., W. Allan, M. S. Ruderman, and R. C. Elphic (2002), The dynamics of current carriers in standing Alfvén waves: Parallel electric fields in the auroral acceleration region, *J. Geophys. Res.*, *107*, 1120.

Wygant, J. R., et al. (2002), Evidence for kinetic Alfvén waves and parallel electron energization at 4-6 R_E altitudes in the plasma sheet boundary layer, *Journal of Geophysical Research (Space Physics)*, *107*, 1201–+, doi:10.1029/2001JA900113.

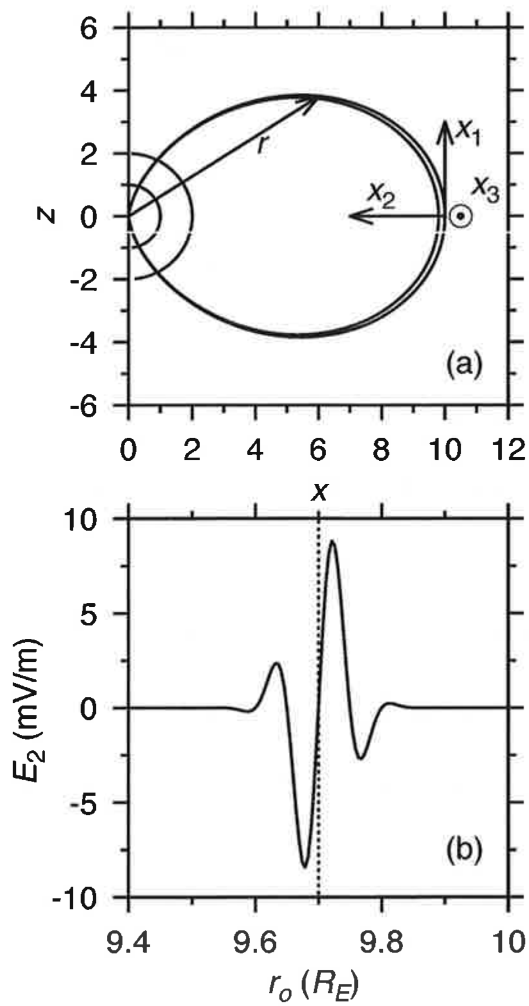

Figure 1. a): Simulation domain where x_3 is positive increasing out of the page. The circles of radius 1 and 2 R_E respectively denote the surface of the Earth and "ionospheric" boundary. The angle θ is subtended from the z axis. After *Damiano et al.* [2007]. b) Initial radial (E_2) electric field profile as a function of r_o at the equator for $L_\perp = 0.1\ R_E$.

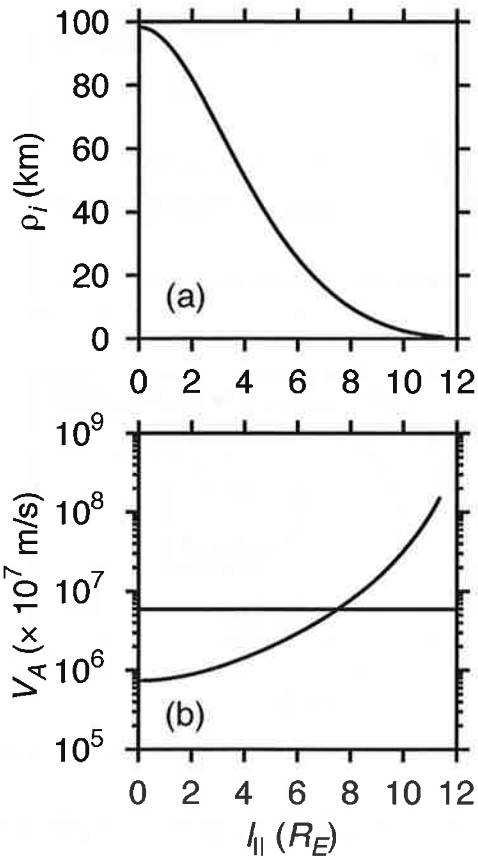

Figure 2. a) Ion gyroradius profile for $T_i = 1$ keV as a function of length along the field line ($l_{||}$) measured from the equator in R_E. b) Alfvén velocity profile as a function of $l_{||}$. The dotted horizontal line denotes $v_{th} = V_A$.

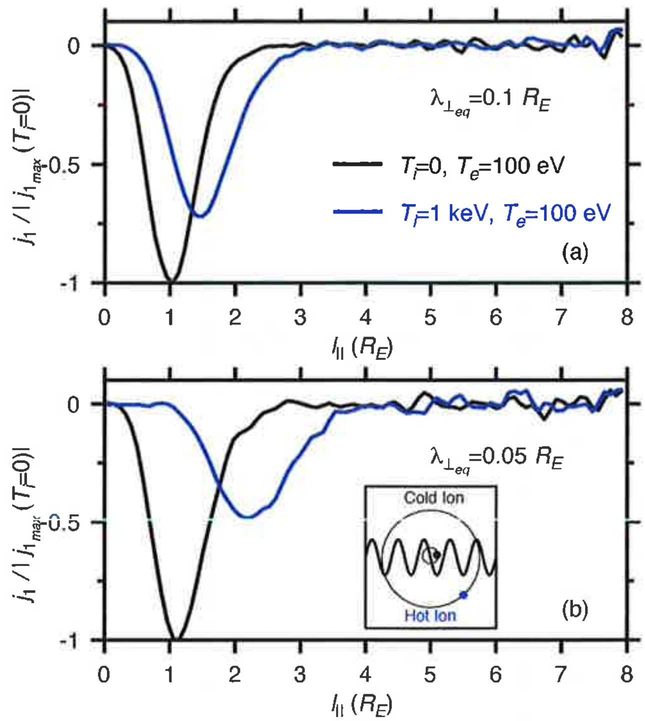

Figure 3. a) Parallel current density along $r_o = 9.7$ field line at $t = 8$ seconds, normalized by the absolute value of the maximum current amplitude in the $T_i = 0$ case, as a function of $l_{||}$. b) Same, but for $\lambda_{\perp_{eq}} = 0.05\ R_E$. Inset: Cartoon of cold and hot ion orbits relative to the perpendicular electric field in a kinetic Alfvén wave. The hot ion feels a smaller orbit averaged perpendicular electric field ($< E_\perp >$) than a cold ion interacting with the same wave.

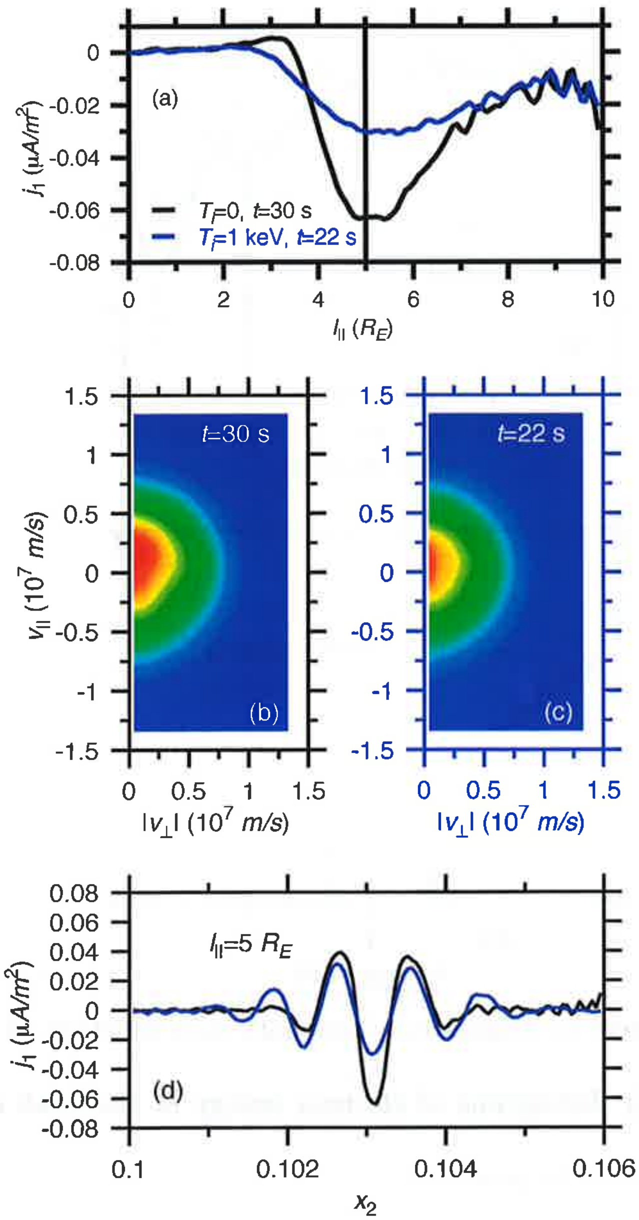

Figure 4. (a) Parallel current density along $r_o = 9.7$ as a function of length along the field line (measured from the equator) for the $T_i = 0$ (black) and $T_i = 1$ keV cases (blue) at indicated times. (b) Distribution function at $l_{||} = 5\ R_E$ (indicated by vertical black line in panel (a)) for case of $T_i = 0$ and $t = 30$ seconds. (c) Same, but for case with $T_i = 1$ keV and $t = 22$ seconds. (d) Perpendicular profile of parallel current density at $l_{||} = 5\ R_E$ at times indicated in panel (a).

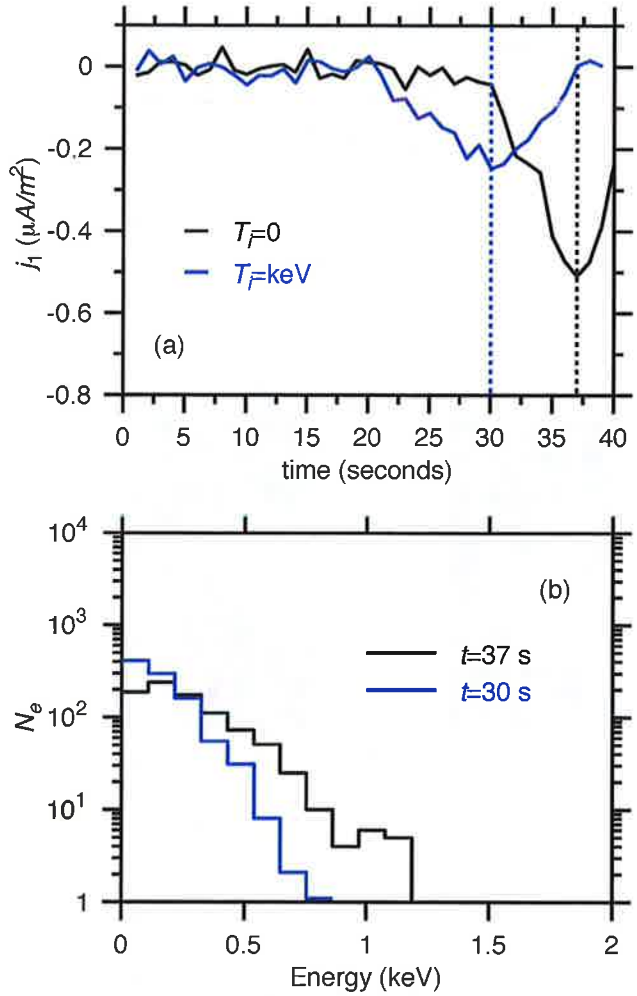

Figure 5. a) Parallel current at ionospheric boundary as a function of time for same parameters as Figure 4a. b) Histograms of electron energy at the peak of the parallel current in each case as indicated in panel (a).

Princeton Plasma Physics Laboratory
Office of Reports and Publications

Managed by
Princeton University

under contract with the
U.S. Department of Energy
(DE-AC02-09CH11466)

P.O. Box 451, Princeton, NJ 08543
Phone: 609-243-2245
Fax: 609-243-2751

E-mail: publications@pppl.gov

Website: http://www.pppl.gov